Vapor-liquid critical and interfacial properties of square-well fluids in slit pores

Cite as: J. Chem. Phys. **130**, 214707 (2009); https://doi.org/10.1063/1.3148884
Submitted: 30 October 2008 . Accepted: 14 May 2009 . Published Online: 04 June 2009

Subimal Jana, Jayant K. Singh, and Sang Kyu Kwak

Vapor-liquid critical and interfacial properties of square-well fluids in slit pores

Subimal Jana,[1] Jayant K. Singh,[1,a)] and Sang Kyu Kwak[2]
[1]*Department of Chemical Engineering, Indian Institute of Technology Kanpur, Kanpur 208016, India*
[2]*Division of Chemical and Biomolecular Engineering, School of Chemical and Biomedical Engineering, Nanyang Technological University, Singapore 637459, Singapore*

(Received 30 October 2008; accepted 14 May 2009; published online 4 June 2009)

Vapor-liquid phase equilibria of square-well (SW) fluids of variable interaction range: $\lambda\sigma=1.25$, 1.75, 2.0, and 3.0 in hard slit pores are studied by means of grand-canonical transition-matrix Monte Carlo (GC-TMMC) simulation. Critical density under confinement shows an oscillatory behavior as slit width, H, reduced from 12σ to 1σ. Two linear regimes are found for the shift in the critical temperature with the inverse in the slit width. The first regime is seen for $H>2.0\sigma$ with linear increase in the slope of shift in the critical temperature against inverse slit width with increasing interaction range. Subsequent decrease in H has little consequence on the critical temperature and it remains almost constant. Vapor-liquid surface tensions of SW fluids of variable well extent in a planar slit pore of variable slit width are also reported. GC-TMMC results are compared with that from slab based canonical Monte Carlo and molecular dynamics techniques and found to be in good agreement. Although, vapor-liquid surface tension under confinement is found to be lower than the bulk surface tension, the behavior of surface tension as a function of temperature is invariant with the variable pore size. Interfacial width, ξ, calculated using a hyperbolic function increases with decreasing slit width at a given temperature, which is contrary to what is being observed recently for cylindrical pores. Inverse scaled interfacial width (ξ/H), however, linearly increases with increase in the scaled temperature $(T_{c,\mathrm{bulk}}-T)/T_{c,\mathrm{bulk}}$. © *2009 American Institute of Physics*.
[DOI: 10.1063/1.3148884]

I. INTRODUCTION

Fluid confined in nanopores is a common occurrence in variety of industrial process such as catalysis, enhanced oil recovery, sensors, and membranes. In such cases, understanding the phase equilibria and having knowledge of structural and transport properties of confined fluids are important in the development of new technologies for manufacturing and in the modification of current methods. Phase behaviors of fluid in porous materials are dramatically different from the bulk fluid because of the competition of fluid-fluid and fluid-wall interaction energies. Moreover, geometry of the adsorbate can make the adsorbent behave as a two dimensional (2D) fluid in nanotubes or one dimensional fluid as for gases stuck in the corners of rectangular pores.[1,2] These geometrical constraints and the presence of external forces are the primary source for different phase transitions such as layering, prewetting, and capillary condensation.[3]

Various experimental works were conducted to understand the capillary condensation in porous materials. For example, experimental studies by Wong and co-workers,[4,5] Burgess *et al.*,[6] De Keizer *et al.*,[7] and Machin[8,9] illustrate that vapor-liquid critical temperature is suppressed under confinement. This decrease in the critical temperature increases with decreasing pore size as a result of decrease in the average coordination number.[10] However, due to wide pore size distribution and irregular pore geometry, it has not been possible earlier to establish a quantitative relation between the pore size and the shift of the vapor-liquid critical point. Nevertheless, in recent years, with the discovery of well-defined geometry of porous materials such as MCM-41,[11] MCM-48, and SBA-15,[12] direct experimental measurements are possible to obtain a quantitative relation between the shift in the vapor-liquid critical temperature and the pore size. For example, capillary critical temperatures in confined geometries are reported experimentally for SF_6 in porous glass and several gases in MCM-41 by Thommes *et al.*[13] and Morishige Findenegg,[14] respectively; the shift in the critical temperature is found to have linear dependence on the inverse pore width. Numerous theoretical studies and molecular simulations including density function theory[15–18] and Monte Carlo (MC) simulations[19–25] were performed to understand capillary condensation. Vishnyakov *et al.*[26] were the first to perform MC simulations systematically on carbon slit pores and studied the shift of the vapor-liquid critical point under confinement. Interestingly, they obtained similar results as seen experimentally; however, the simulations were limited to five molecular diameters pore size. Recent work of Vortler[27] on a square-well (SW) fluid in a hard slit-pore suggests, on the other hand, nonlinear dependence of the shift in the critical temperature as a more generic behavior in nanopores for variable pore sizes. As focused on variable pore size in the aforementioned works, there are other studies pertaining to the effect of wall-fluid interaction on the

a)Author to whom correspondence should be addressed. Electronic mail: jayantks@iitk.ac.in.

critical temperature. For example, Zhang and Wang,[28] in their recent study, found that the shift in the critical temperature varies nonmonotonically with the variation in the wall-fluid interaction strength. Similar results were observed for SW fluid in slit pores in our previous work.[29] On the other hand, recent works on disordered and interconnected pores and narrow cylindrical pores have shown that capillary condensation cannot be considered as the first order transition,[30] which led to some debate.[16,17,23,31]

The critical temperature estimation is an integral part in the calculation and understanding of phase equilibria, yet little work has been reported on the effect of fluid-fluid interaction range on phase equilibria and critical properties under confinement. In this sense, composite effects of variable pore size with variable interaction range are somewhat missed from the far-reaching comprehension on the vapor-liquid critical temperature under confinement. Therefore, we first aim to calculate critical properties of SW fluids confined in slit pores from 12 to 1 molecular diameter pore size and analyze the behavioral change in the shift in critical properties for variable fluid-fluid interaction range. Although, fluid-wall tension has been investigated by various authors,[32,33] vapor-liquid interfacial properties under confinement have not been studied well. In our previous study,[29] we examined different approaches to evaluate the surface tension under confinement. Following the prescribed scheme in the previous work,[29] our second aim is to investigate the surface tension, interfacial width, and structural properties of coexistence phases of variable SW fluids in variable slit pores.

The paper is outlined as follows. Section II describes the potential model, thermodynamics of surface tension under confinement, and simulation methodology used in this work with simulation details. The results are systematically discussed in Sec. III, which is followed by a summary in Sec. IV.

II. SIMULATION MODEL AND METHODS

In this work, fluid-fluid interaction is represented by the SW potential,

$$u_{f-f}(r_{ij}) = \begin{cases} \infty, & 0 < r_{ij} < \sigma, \\ -\varepsilon, & \sigma \le r_{ij} < \lambda\sigma, \\ 0, & \lambda\sigma \le r_{ij}, \end{cases} \tag{1}$$

where $\lambda\sigma$ is the potential-well diameter, ε is the depth of the potential well, and σ is the diameter of the hard core. SW model was introduced originally to understand simple liquid;[34] however, due to its analytic tractability it has become even more useful for colloidal system,[35–37] heterochain molecules,[38–40] and complex system,[41–43] among others.

Fluid-wall interaction is also represented by the hard potential,

$$u_{w-f}(r) = \begin{cases} \infty, & r < \sigma/2.0, \\ 0, & \sigma/2.0 \le r. \end{cases} \tag{2}$$

We adopt units such that ε and σ are unity. Reduced units used in this study are temperature $T^* = kT/\varepsilon$, density $\rho^* = \rho\sigma^3$, pressure $P^* = P\sigma^3/\varepsilon$ and surface tension $\gamma^* = \gamma\sigma^2/\varepsilon$.

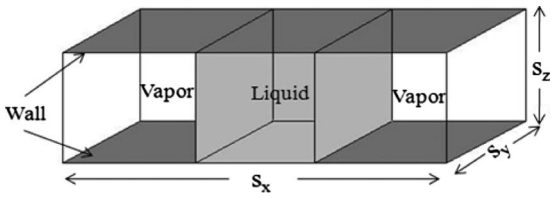

FIG. 1. Diagram of simulation box with vapor and liquid coexistence under slit pore confinement of slit width, $H=s_z$.

The fundamental equation of a fluid confined in a slit pore, as shown in Fig. 1, is given as[32,33]

$$dF = -SdT + \mu dN - p_{xx}s_y s_z ds_x - p_{yy}s_x s_z ds_y - p_{zz}s_x s_y ds_z, \tag{3}$$

where F is the Helmholtz free energy, S is the entropy, T is the temperature, μ is the chemical potential, N is the amount of the fluid, s_i is the thickness of the fluid in the direction of i, and p_{ii} is the iith component of the pressure tensor.

For the geometry as described in Fig. 1, the volume of the simulation box is $V=s_x s_y s_z$, the slit width is defined as $H=s_z$, the length of the simulation box in the direction perpendicular to the vapor-liquid interface is s_x, and interfacial area of vapor-liquid interface in the simulation box is $A'=2Hs_y$. With the following variables $R=s_x/s_y$, $A=s_x s_y$, $\gamma_1=-(p_{xx}+p_{yy})s_z/2$, and $\gamma_2=(p_{yy}-p_{xx})s_z/2R$, the above equation can be rewritten as

$$dF = -SdT + \mu dN + \gamma_1 dA + \gamma_2 A dR - p_{zz}A ds_z. \tag{4}$$

In this work, slit width H is kept constant. Hence, at a constant T, N, and substrate area A, we get the following expression:

$$\left(\frac{\partial F}{\partial R}\right)_{T,N,s_z,A} = \left(\frac{\partial F}{\partial R}\right)_{T,N,V} = \gamma_2 A. \tag{5}$$

A simple mathematical manipulation of the above equation with $L=s_x$ leads Eq. (5) to[29]

$$\left(\frac{\partial F}{\partial A'}\right)_{T,N,V} = -\frac{\gamma_2 AL}{Hs_y^2} = \frac{L(p_{xx}-p_{yy})}{2} = \gamma_{v-l}, \tag{6}$$

where P_{xx} is the spreading pressure, parallel to the wall and perpendicular to the interface, P_{yy} is the pressure component parallel to the interface and the wall, and γ_{v-l} is the vapor-liquid surface tension. The division factor of 2 in the above formula accounts for the presence of two interfaces in the system.

Pressure-tensor components are obtained from the virial formalism,[44] which for pairwise-additive potential, is expressed as

$$p_{\alpha\beta} = \rho k_B T + \frac{1}{V}\left\langle \sum_{i=1}^{N-1}\sum_{j>i}^{N} (\mathbf{r}_{ij})_\alpha (\mathbf{f}_{ij})_\beta \right\rangle, \tag{7}$$

where ρ is the number density N/V, $\mathbf{r}_{ij}$ is the vector between the center of mass of molecules i and j, and $\mathbf{f}_{ij}=-\nabla u_{ij}$ is the force between them; the angle brackets indicate the ensemble or time average.

Equation (7) can be evaluated using both MC and molecular dynamics (MD) techniques. In MC simulation, we calculated the force using the step function Θ,[45]

$$(f_{ij})_\beta = k_B T\left(\frac{\Theta(r-\sigma)-\Theta(r-\sigma-\Delta\sigma)}{\Delta\sigma}\right)\left(\frac{(r_{ij})_\beta}{r}\right). \quad (8)$$

The above equation is valid in the limit of $\Delta\sigma$ goes to 0. Using the step function the expression for pressure components, P_{xx} and P_{yy}, for a SW fluid can be written as follows:

$$p_{\alpha\beta} = \rho k_B T + p_{\alpha\beta}(\sigma^+) + p_{\alpha\beta}(\lambda\sigma^-) + p_{\alpha\beta}(\lambda\sigma^+), \quad (9)$$

where $p_{\alpha\beta}(\sigma^+)$, $p_{\alpha\beta}(\lambda\sigma^-)$, and $p_{\alpha\beta}(\lambda\sigma^+)$ represent the contribution from the hard core and square well and are calculated using Eqs. (7) and (8).

Pressure components in canonical ensemble (NVT) MC simulations were calculated using Eqs. (7)–(9). In this work, we used $\Delta\sigma/\sigma$=0.005, 0.010, 0.015, and 0.020 to obtain the pressure components. Pressure at the limit of $\Delta\sigma\to 0$ is obtained by extrapolating results at various nonzero $\Delta\sigma$.

In MD simulation, collision dynamics is implemented to calculate the pressure tensor and consequently surface tension. For discontinuous potential such as those used in this study, the forces are impulsive, having infinite magnitude but acting for an infinitesimal time. When integrated over time each collision contributes a well-defined amount to the average in the following expression:

$$p_{\alpha\beta} = \rho k_B T + \frac{1}{V t_{\text{sim}}} \sum_{\text{collisions}} (\mathbf{r}_{ij})_\alpha (\Delta\mathbf{p}_{ij})_\beta, \quad (10)$$

where t_{sim} is the total simulation time and the sum is over all collisions occurring in this time; $\Delta\mathbf{p}_{ij}$ is the change in momentum associated with the collision between molecules i and j.

Phase transition under confinement in this work is studied by GC-TMMC.[29,46] In this approach, MC simulations are conducted in a standard grand canonical ensemble where the volume (V), chemical potential (μ), and temperature (T) are held constant and the particle number N (or density) and energy (U) fluctuates. During a simulation, attempted transitions between states of different densities are monitored. At regular intervals during a simulation, this information is used to obtain an estimate of the density probability distribution, which is subsequently used to bias the sampling to low probability densities. Over time, all densities of interest are sampled adequately. The result is an efficient self-adaptive method for determining the density probability distribution over a specified range of densities (typically a range that corresponds to the densities of two potentially coexisting phases). Once a probability distribution has been collected at a given value of chemical potential (μ_0), histogram reweighting[47] is used to shift the probability distribution to other values of the chemical potential using the following relation:

$$\ln \prod(N,\mu) = \ln \prod(N,\mu_0) + \beta(\mu-\mu_0)N. \quad (11)$$

To determine the coexistence chemical potential, we apply the above relation to estimate the chemical potential that produces a coexistence probability distribution. Saturated densities are related to the first moment of the vapor and liquid peaks of the coexistence probability distribution, $\Pi_c(N)$. To calculate the saturation pressure we use the following expression:

$$\beta PV = \ln\left(\sum \prod_C (N)/\prod_C (0)\right) - \ln(2). \quad (12)$$

GC-TMMC along with finite size scaling analysis of Binder[48] can also be used to find the surface tension of vapor-liquid under confinement as demonstrated in our earlier work.[29] The interfacial free energy of a 2D surface (with area $A=LH$) can be expressed with the system size according to Binder's formalism and is given by

$$\beta\gamma_L = \frac{\beta F_L}{2A} = C_1\frac{1}{A} + C_2\frac{\ln L}{A} + \beta\gamma_\infty, \quad (13)$$

where γ_L is an apparent system-size-dependent surface tension, γ_∞ is the true infinite-system ($L\to\infty$) interfacial tension, and C_1 and C_2 are constants. The method enables one to evaluate the infinite-system interfacial tension by extrapolating a series of finite-system interfacial free energies.

GC-TMMC has been applied recently for variety of systems,[29,49–54] mainly due to the ease of utilizing parallel processors and efficiency over GEMC.[55] In this work, we applied GC-TMMC to evaluate the phase coexistence data of variable SW fluid of interaction range λ=1.25, 1.75, 2.0, and 3.0. Grand-canonical simulations are conducted with 30% displacement, 35% insertion, and 35% deletion moves. For phase coexistence calculation, the box length is varied from $L\sim 8$ to 28 depending on the slit width. To calculate the surface tension using GC-TMMC and finite size scaling, we performed simulations for different box lengths varying from $L\sim 14$ to 41 for a given slit width. The technique is described in detail by Errington.[56] Four independent runs were conducted to calculate the statistical error. These simulations were run without discarding any transition matrix probabilities[46] on two quadcore processors from 2 to 12 h depending on the system size.

In this work, we estimated the critical parameters by using the coexistence data and the least squares fit of the following scaling law:[57]

$$\rho_l - \rho_v = C\left(1-\frac{T}{T_C}\right)^{\beta_C}, \quad (14)$$

where ρ_l and ρ_v are coexistence liquid and vapor number densities, respectively, and C and β_c are fitting parameters. The critical temperature, T_C, estimated from Eq. (14) is used to calculate the critical density, ρ_c, from the least squares fit of the following equation:

$$\frac{\rho_l+\rho_v}{2} = \rho_c + D(T-T_C), \quad (15)$$

where D is a fitting parameter.

The slab-based molecular simulation technique is used to determine the density profile at the interface of the coexisting vapor and liquid phases. MD simulations are conducted in the canonical ensemble with N=2000 particles, where the liquid phase is present as a slab of the simulation box in coexistence with the vapor phase filling up the rest of

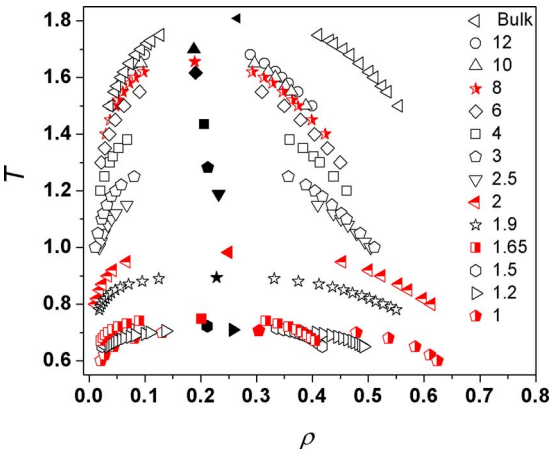

FIG. 2. (Color online) Phase coexistence envelope of a SW fluid with well extent 1.75 in slit pores of various slit widths. Filled symbol indicates critical temperature. Legends represent the slit width of the pore. The error bars are smaller than the symbol size.

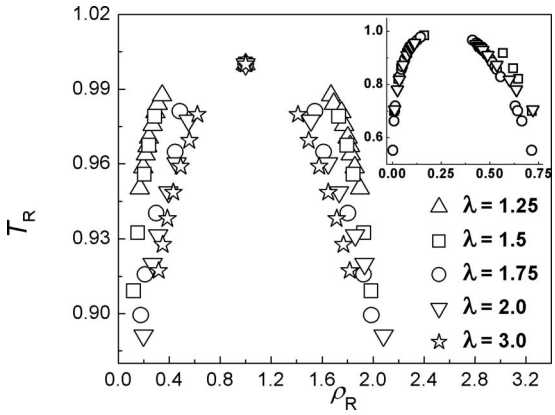

FIG. 3. Corresponding state plot of reduced temperature against reduced density under confinement of slit width, $H=2.5$, for SW fluids of various fluid-fluid interaction range. The inset represents the bulk corresponding state plot of reduced temperature against reduced density for SW fluids of different fluid-fluid interaction range. The error bars are smaller than the symbol size.

the simulation cell. There are two vapor-liquid interfaces in the simulation box due to periodic boundary conditions applied. The reduced time step Δt^* (in units of $\sigma\sqrt{m/\varepsilon}$) is fixed at 0.04. We have taken 10^5 time steps as equilibration period and equal number for production steps.

Density profile obtained from NVT simulations is fitted to the following expression to evaluate the interfacial width:[45]

$$\rho(z) = \frac{1}{2}(\rho_l + \rho_v) - \frac{1}{2}(\rho_l - \rho_v)\tanh\left(\frac{2(z-z_0)}{\delta}\right), \qquad (16)$$

where ρ_v and ρ_l are coexisting densities of vapor and liquid phases, δ is the interfacial width, and z_0 is the position for Gibbs dividing surface.

III. RESULTS AND DISCUSSION

A. Phase diagram under confinement

We start our discussion with the effect of confinement on vapor-liquid critical temperature and density, which is shown in Fig. 2 for a SW fluid with well extent 1.75. The effect of confinement of repulsive nature on the critical density is similar to that of the critical temperature, i.e., confinement suppresses the critical density as seen for $H=12.0$; however, it is found to increase with decreasing slit width until $H=2.0$. Such behavior is completely reversed for extremely narrow slit width, $2.0 \leq H < 1.5$, where critical density is found to decrease with reducing slit width. Subsequent decrease in the slit width led critical density to increase and approach the 2D value. It is worth noting that critical temperatures in slit pores, $H=1.5$, 1.2, and 1.0, are nearly the same. The critical temperature in slit pore $H=1.5$ is within 2% of the 2D value. Although, there is density variation in the vapor and liquid phases for the above mentioned slit-pore system, the system can accommodate only one layer of molecules under such confinement. In fact, for the above set of slit widths, densities of both the liquid and vapor phase increase with decreasing H leading to almost constant critical temperature. Similar behavior is observed for $\lambda=1.5$ and 3.0. On the other hand, we noticed that for $\lambda=1.25$, vapor-liquid phase transition under confinement is extremely difficult to obtain for pore size smaller than $H=2.0$, due to the shrinkage of temperature range for such phase transition, which may exist for extremely narrow pores. A more concerted effort would be needed for investigating extremely low interaction range $\lambda <= 1.25$ in ultrananopores, which is kept for a future study.

The critical density at $H=12$ is significantly less than that of the bulk as seen in Fig. 2, but it is apparent that critical density should approach the three dimensional (3D) value with the increase in H beyond 12. One can explain the behavior by looking at the density of the saturated gas and liquid. The fractional density change in the pore with $H=12$, $(\rho_{\text{bulk}}-\rho_{\text{confined}})/\rho_{\text{confined}}$, for saturated gas and liquid are 9% and 39%, respectively, at $T=1.5$. These values indicate that with the increase in the slit width beyond $H=12$, critical density should bottom out at certain higher H, and subsequently should rise again toward the bulk density. Similar behavior is observed for different interaction ranges, $\lambda=1.25$, 1.50, 1.75, and 3.0. In this work, vapor-liquid coexistence data of the confined SW fluid with $\lambda=1.50$ and bulk critical properties of SW fluids are taken from the literature.[29,49,57,58]

To understand the effect of long range interaction on phase equilibria of SW fluids under confinement, we investigated the nature of corresponding state plot in bulk and in slit pores, which is obtained by scaling temperature and density using the corresponding critical temperature and density for different fluid-fluid well-extents. Figure 3 presents the corresponding state plot of the bulk and confined fluids. The corresponding state plot of the bulk fluid unambiguously indicates that the saturation gas curve is invariant to the change in the interaction range of the fluid. However, the saturation liquid curve significantly varies with the change in the interaction range particularly at lower temperatures. Notably, coexistence envelopes of $\lambda=1.75$ and 2.0 are found to shrink compared to that of $\lambda=1.5$. Interestingly, this behavior is accentuated under confinement as reflected in Fig. 3. Saturation curves, in the corresponding plot, are observed not to

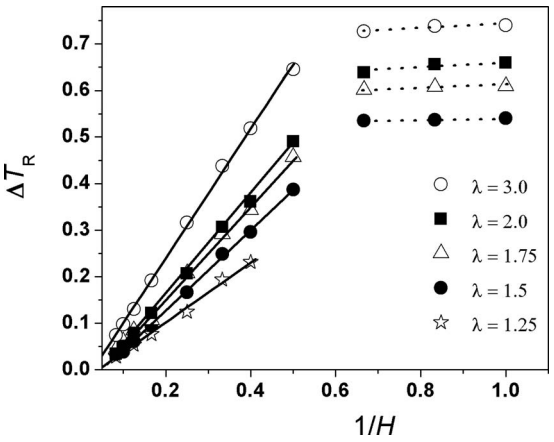

FIG. 4. Fractional critical temperature shift against inverse slit width for different fluid-fluid well extents. The error bars are smaller than the symbol size.

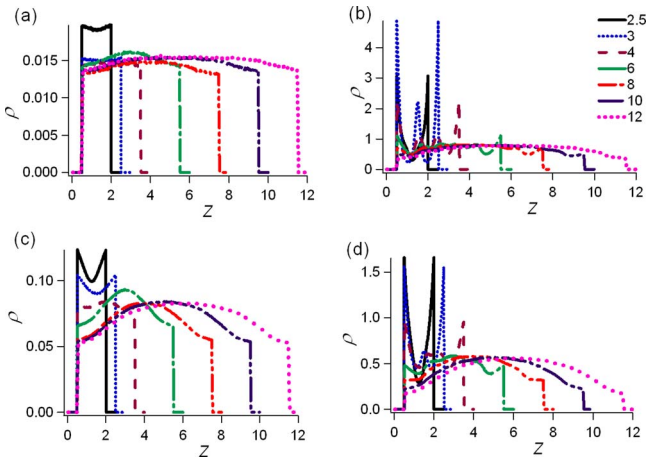

FIG. 5. (Color online) Density profile of a SW fluid with λ=3.0 in slit pores of various slit widths: (a) and (b) correspond to the vapor and liquid phases, respectively, at T_R=0.7; (c) and (d) correspond to the vapor and liquid phases, respectively at T_R=0.9. The error bars are smaller than the linewidth.

fall on a master curve as seen for bulk fluids; rather the behavior is distinct for different fluid-fluid interaction ranges under confinement. Hence, it is clear from the corresponding plot that these fluids behave differently from each other under confinement.

We performed extensive simulations for various fluid-fluid interaction ranges and slit widths to investigate the shift in the capillary critical temperature, $\Delta T_{cr}=(T_{c,bulk}-T_{c,pore-})/T_{c,bulk}$. The critical property data, obtained in this work, are available electronically (EPAPS).[59] It was noted by earlier investigators[13,14,26] that ΔT_{cr} is inversely proportional to the pore size. Those studies, however, were limited to the pore size of few molecular diameters. On the other hand, a recent work of Vortler[27] suggests a generic, an exponential relation, though empirical, for the complete range of slit widths. Figure 4 presents a plot of ΔT_{cr} against inverse slit width for various well extents. ΔT_{cr} is found to have a linear relation from H=12 until H=2.5 for λ=3.0; whereas for smaller attraction range, λ=1.75 and 1.5, linear regime is seen until H=2.0. We observe that critical temperature for H=1.0 does not fall in the same linear regime, akin to Vortler's observation.[27] The effect of confinement is more prominent for fluid with larger interaction range. We note that the critical temperature remains almost constant for pore size less than 1.5 to such an extent that it may look that two dimension behavior is extended up to H=1.5. The second linear regime in the critical temperature is established for all fluid-fluid well extents except for 1.25, for which we found it extremely difficult to search for the vapor-liquid transition in pores with $H<2.5$. We have also recently shown that such two linear regimes for the shift in the critical temperature in slit pores generally holds for normal alkanes.[60]

We further studied the structural behavior of the coexisting phases to understand the behavioral change in the critical temperature shift. Figures 5(a) and 5(b) present the density profile of the coexistence vapor and liquid phases for the fluid interaction range λ=3.0 at a reduced temperature, $T_R=T/T_{c,pore}$=0.7, for various slit pores. Uniform density profiles in the liquid and vapor phases, in the center of the pore, prevail in large pores. The sticking tendency of molecules (e.g., away from the hard walls) is much more prominent in large pores, which leads to depletion of particles near the surface. However, in narrow pores due to the lack of available volume for molecules to move around, the depletion is invisible and instead we observe a layering behavior. Such layering behavior is visibly depicted in the density profile of the liquid phase for H=4. On the contrary, the density profile of the vapor phase in the slit pore of width H=4 still reflects more uniform density; though, molecules are accumulated relatively more in the center of the pore. However, further decrease in the pore size vanishes the hump in the density profile of the vapor phase; instead, two layers of higher density appear in the pore width H=2.5. In the liquid phase, for slit widths less than 4.0, peak density of layers in the density profile approaches a maximum around H=3.0 and, subsequently, it reduces with decreasing slit width as seen for H=2.5.

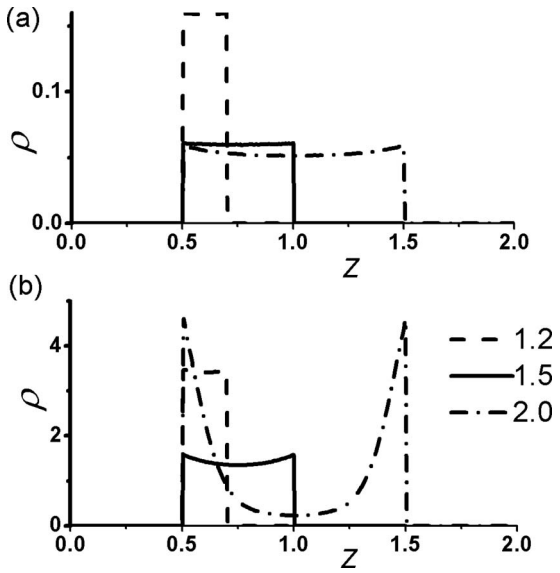

FIG. 6. Density profile of a SW fluid with λ=1.50; (a) and (b) correspond to the vapor and liquid phases, respectively, at T_R=0.9 for different slit pores. The error bars are smaller than the linewidth.

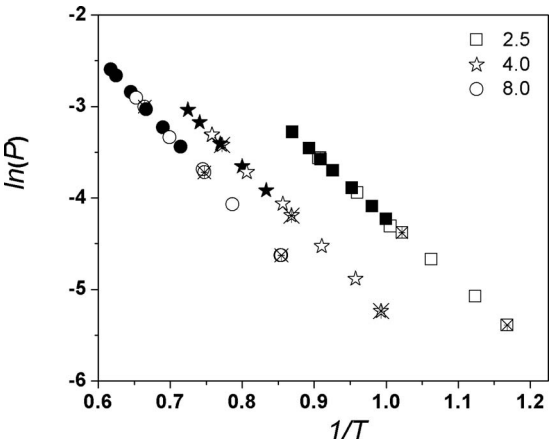

FIG. 7. $\ln(P)$ vs $1/T$ of a SW fluid with $\lambda=1.75$. Open, filled, and crossed systems are results of MD, GCMC, and NVT-MC, respectively. The error bars are smaller than the symbol size.

The behavior at a higher temperature $T_R=0.9$ as shown in Figs. 5(c) and 5(d) is similar in nature to that seen in Figs. 5(a) and 5(b), except that the vapor phase density is higher and layering behavior is seen even in the vapor phase at lower slit widths. For smaller fluid-fluid interaction range, $\lambda=1.25$, similar behavior is seen (figure not shown). From Fig. 5, it is apparent that the liquid phase packing in the slit pore with $H=3.0$, at the same reduced temperature, is higher than that in a narrower pore, $H=2.5$. Surprisingly, such behavior is seen only in the liquid phase and is invariant to temperature and interaction range. This is due to the geometrical constraint, which allow molecules to pack more in the pore with $H=3$ compared to that in the pore with $H=2.5$. We notice in Fig. 2 that critical density attained two minima and one local maximum in between the bulk and the 2D fluid. In particular, the decrease in the critical density from $H=2.0$ onwards until $H=1.5$ and subsequent increase toward a 2D value is intriguing. To gain further insight into this fascinating nature, we studied the density profile in pores of widths $H=2.0$, 1.5, and 1.2. Figure 6 presents a plot of a SW fluid at $T_R=0.7$, which clearly illustrates a drastic change in the coexisting liquid phase in the aforementioned slit

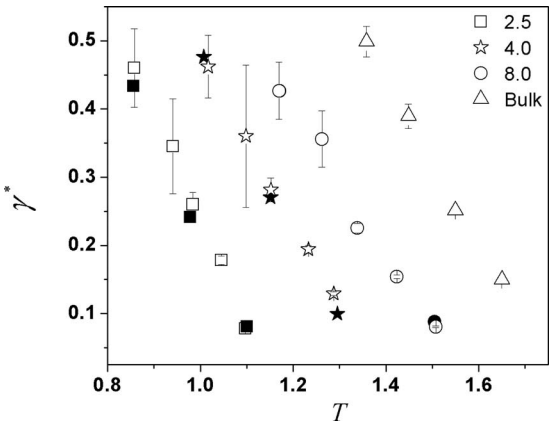

FIG. 8. Surface tension against reduced temperature in slit pores of various slit widths of a SW fluid with $\lambda=1.75$. Open symbols are the MD results. Filled symbols are the values obtained from GC-TMMC simulations. The error bars (where not visible) are smaller than the symbol size.

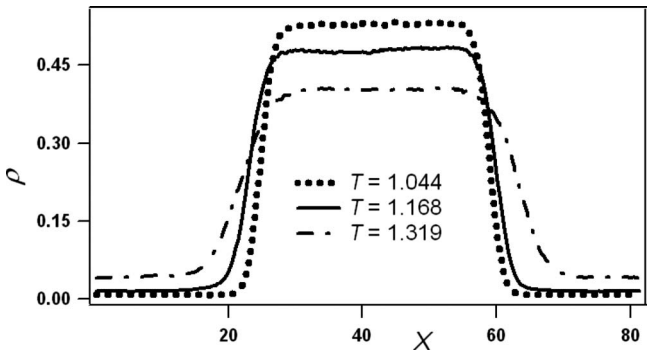

FIG. 9. Density profile from MD simulation of a SW fluid with $\lambda=1.75$ and slit width $H=8$ at various temperatures. The error bars are smaller than the linewidth.

pores. In the pore with $H=2.0$, two peaks are visibly present, which are missing in pores with $H=1.5$ and 1.2. This is attributed to the reduction in space for any possibility of layering behavior. The density profile also clearly indicates the decrease in the liquid density for $H=1.5$ compared to that seen in the pore with $H=2.0$. Vapor density on the other hand does not change significantly in pores with $H=2.0$ and 1.5. Hence, saturated liquid curve shifts toward left for slit widths in the range of 1.5 and 2.0, leading to the decrease in the critical density. Further reduction in the slit width increases the corresponding liquid density as well as vapor density; however, increase in the density of the liquid phase is significantly higher. In effect, these changes reverse the behavior of critical density for $H<1.5$ as seen in Fig. 2.

B. Vapor-liquid interfacial tension under confinement

One of the major objectives of this work is to obtain the surface tension of SW fluids for variable interaction range using different methods. To calculate vapor-liquid surface tension, we can use either Eq. (13) or a mechanical definition-based formula as shown in Eq. (6). In the latter, NVT-MD and NVT-MC with application of the delta function are suitable. Figure 7 presents the comparison of saturation pressure evaluated from GC-TMMC, NVT-MD, and NVT-MC+delta function. Note that saturation pressure (pressure component parallel to the surfaces) using NVT-MD and NVT-MC+delta function are calculated for the vapor phase. The number density is taken from the coexistence value obtained from GC-TMMC simulations. Comparison is excellent for single phase system under confinement. However, for two phase simulations, we found it difficult to obtain reasonable estimates of pressure components via NVT-MC+delta function. Although the equilibrium pressure (in the direction perpendicular to the vapor-liquid interface) is obtained within few thousand simulation cycles and is reasonable accurate for different ranges of delta values, transverse pressure, p_{yy}, is extremely sensitive to the range of delta values. Since the difference in the values of p_{xx} and p_{yy} is very low at moderate temperatures, high precision simulations are required for the calculation of pressure tensor under confinement, particularly, for the estimation of surface tension. Figure 8 presents the surface tension of SW fluid

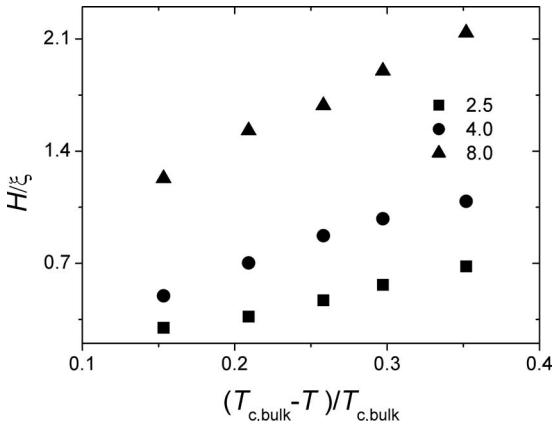

FIG. 10. Scaled interfacial width against scaled temperature of a SW fluid with $\lambda=1.75$ for different slit widths. The error bars are smaller than the symbol size.

with well extent 1.75 under confinement, calculated using GC-TMMC and MD techniques; results are in good agreement. Akin to the bulk vapor-liquid surface tension, the values under confinement decreases with increasing temperature and is found to be linear in nature. Increase in the slit width induces a systematic increase in the surface tension at the same temperature. Similar behavior is observed for $\lambda=1.25$ and 3.0.

Surface tension is invariably related to the interfacial width, ξ, or thermal fluctuation of the interface.[61] For example, Kuo *et al.*[62] used tan-hyperbolic function to fit the density profiles for various water models. On the other hand, Sides *et al.*[63] and Ismail *et al.*[64] used both tan-hyperbolic and error function for the Lennard-Jones fluid and various water models, respectively, and obtained the interfacial width. In this work, we investigate the vapor-liquid interfacial width for different temperatures and various degrees of confinement by fitting the tan-hyperbolic function to the vapor-liquid density profile obtained from NVT simulations as shown in Fig. 9 for $\lambda=1.75$. These data together with surface tension values are available electronically.[59] The vapor-liquid density profile under confinement is akin to the bulk behavior,[65] i.e., increase in the temperature decreases the sharpness or increases the interfacial width and it diverges as the temperature approaches the critical value. Increase in the slit width decreases the interfacial width at a constant temperature, which is surprisingly opposite in the cylindrical pore.[66] However, the reason for such an anomaly in the cylindrical pores is still unclear. Interestingly, the inverse of the scaled interfacial width, ξ/H, linearly increases with the increase in the shift in the temperature, $(T_{c,\mathrm{bulk}}-T)/T_{c,\mathrm{bulk}}$, as shown in Fig. 10. The slope of the curve, however, is directly related to the pore size and is found to increase with increasing pore size. As temperature approaches the bulk critical temperature (which would be case for extremely large pore), H/ξ should approach zero. However, Fig. 10 suggests that H/ξ for $H=8.0$, 4.0, and 2.5 does not tend to zero as temperature approaches $T_{c,\mathrm{bulk}}$, which indicates a different scaling relation for large pore sizes and at higher temperatures.

C. Critical exponents: Crossover from 3D to 2D

Critical exponent β related to the order parameter is found to decrease from the 3D Ising ($\sim$0.325) value to 2D Ising value (1/8) with decreasing H. However, the system size effect is significant, particularly, for extremely narrow pores. For example, increasing the maximum number of particles $N_{\max}$, from 1000 to 3500, in the phase equilibria calculation decreases β obtained in the pore with $H=8$ by 10%. On the other hand, for $H=2$ system, increasing $N_{\max}$ from 800 to 2800 particles decreases β by 19%. On the contrary, critical temperature and critical density are relatively insensitive to system size greater than 1000 particles, as taken in this work.

We also analyzed other critical exponents such as exponent ν related to the correlation length and found that it remains within the range of 3D Ising ($\sim$0.63) and 2D Ising (1.0) values with no clear indication of crossover. We attribute this to limited surface tension or correlation length data, which are calculated for $T/T_{c,\mathrm{pore}}<0.9$. We believe that with mixed field finite size scaling approach,[67] a separate study to understand the crossover of critical exponents from 3D to 2D value under confinement is more appropriate to make a remark, confidently, on the crossover nature of critical exponents.

IV. CONCLUSIONS

We investigated in this work the influence of pore size, ranging from 12 to 1 molecular diameter, on the shift in the vapor-liquid critical temperature of variable SW fluids. In contrast with previous estimations, the dependence of the shift in the critical temperature under confinement of repulsive nature is found to follow two linear regimes. The first linear regime is until $H=2.0$ for $\lambda=1.5$, 1,75, and 2.0. For $\lambda=3.0$, the first linear regime truncates at a slit width slightly higher than 2.0. Subsequent decrease in the slit width leads to almost constant value of the critical temperature Corresponding state plots reveal that the effect of interaction range is more accentuated under confinement, where it is found that segregation based on the interaction range occurs. Surface tensions for all the fluid-fluid interaction ranges are found to be lower than their corresponding bulk value; however, the linear behavior of surface tension against the temperature remains intact under confinement. Interfacial width nonlinearly increases with increasing temperature for SW fluids under confinement, which is akin to the behavior seen for bulk fluids. However, ξ/H is found to increase linearly with the increase in the scaled shift in the temperature, $(T_{c,\mathrm{bulk}}-T)/T_{c,\mathrm{bulk}}$, for small pore size. It is yet to be seen if the above relation holds for larger pore with $H>12$ and temperature closer to the bulk critical temperature.

ACKNOWLEDGMENTS

This work is supported by the Department of Science and Technology (Grant No. SR/S3/CE10/2006) and the Department of Atomic Energy, Govt. of India (Grant No. 2006/20/36/05-BRNS).

[1] M. J. Bojan and W. A. Steele, Carbon **36**, 1417 (1998).
[2] G. M. Davies and N. A. Seaton, Carbon **36**, 1473 (1998).
[3] L. D. Gelb, K. E. Gubbins, R. Radhakrishnan, and M. S. Bartkowiak, Rep. Prog. Phys. **62**, 1573 (1999).
[4] A. P. Y. Wong and M. H. W. Chan, Phys. Rev. Lett. **65**, 2567 (1990).
[5] A. P. Y. Wong, S. B. Kim, W. I. Goldburg, and M. H. W. Chan, Phys. Rev. Lett. **70**, 954 (1993).
[6] C. G. V. Burgess, D. H. Everett, and S. Nuttall, Pure Appl. Chem. **61**, 1845 (1989).
[7] A. De Keizer, T. Michalski, and G. H. Findenegg, Pure Appl. Chem. **63**, 1495 (1991).
[8] W. D. Machin, Langmuir **15**, 169 (1999).
[9] W. D. Machin, Phys. Chem. Chem. Phys. **5**, 203 (2003).
[10] T. L. Hill, *Statistical Mechanics, Principles and Selected Applications* (McGraw-Hill, New York, 1956).
[11] C. T. Kresge, M. E. Leonowicz, W. J. Roth, J. C. Vartuli, and J. S. Beck, Nature (London) **359**, 710 (1992).
[12] D. Y. Zhao, J. L. Feng, Q. S. Huo, N. Melosh, G. H. Fredrickson, B. F. Chmelka, and G. D. Stucky, Science **279**, 548 (1998).
[13] M. Thommes and G. H. Findenegg, Langmuir **10**, 4270 (1994).
[14] K. Morishige and M. Shikimi, J. Chem. Phys. **108**, 7821 (1998).
[15] P. A. Monson, Langmuir **24**, 12295 (2008).
[16] E. Kierlik, P. A. Monson, M. L. Rosinberg, and G. Tarjus, J. Phys.: Condens. Matter **14**, 9295 (2002).
[17] F. Detcheverry, E. Kierlik, M. L. Rosinberg, and G. Tarjus, Phys. Rev. E **68**, 061504 (2003).
[18] F. Detcheverry, E. Kierlik, M. L. Rosinberg, and G. Tarjus, Phys. Rev. E **72**, 051506 (2005).
[19] J.-C. Liu and P. A. Monson, Langmuir **21**, 10219 (2005).
[20] H.-J. Woo and P. A. Monson, Phys. Rev. E **67**, 041207 (2003).
[21] H.-J. Woo, F. Porcheron, and P. A. Monson, Langmuir **20**, 4743 (2004).
[22] J.-M. Pellenq, B. Rousseau, and P. E. Levitz, Phys. Chem. Chem. Phys. **3**, 1207 (2001).
[23] R. J.-M. Pellenq, B. Coasne, R. O. Denoyel, and O. Coussy, Langmuir **25**, 1393 (2009).
[24] I. Brovchenko, A. Greiger, and A. Oleinikova, J. Chem. Phys. **120**, 1958 (2004).
[25] M. Alvarez, D. Levesque, and J. J. Weis, Phys. Rev. E **60**, 5495 (1999).
[26] A. Vishnyakov, E. M. Piotrovskaya, E. N. Brodskaya, E. V. Votyakov, and Y. K. Tovbin, Langmuir **17**, 4451 (2001).
[27] H. L. Vortler, Collect. Czech. Chem. Commun. **73**, 518 (2008).
[28] X. Zhang and W. Wang, Phys. Rev. E **74**, 062601 (2006).
[29] J. K. Singh and S. K. Kwak, J. Chem. Phys. **126**, 024702 (2007).
[30] R. Evans, J. Phys.: Condens. Matter **2**, 8989 (1990).
[31] E. Kierlik, P. A. Monson, M. L. Rosinberg, L. Sarkisov, and G. Tarjus, Phys. Rev. Lett. **87**, 055701 (2001).
[32] D. J. Diestler, M. Schoen, J. E. Curry, and J. H. Cushman, J. Chem. Phys. **100**, 9140 (1994).
[33] D. J. Diestler and M. Schoen, J. Chem. Phys. **104**, 6784 (1996).
[34] J. A. Barker and D. Henderson, Rev. Mod. Phys. **48**, 587 (1976).
[35] P. Bolhuis and D. Frenkel, Phys. Rev. Lett. **72**, 2211 (1994).
[36] N. Asherie, A. Lomakin, and G. B. Benedek, Phys. Rev. Lett. **77**, 4832 (1996).
[37] M. G. Noro and D. Frenkel, J. Chem. Phys. **113**, 2941 (2000).
[38] J. Cui and J. R. Elliot, J. Chem. Phys. **114**, 7283 (2001).
[39] C. McCabe, A. Gil-Villegas, G. Jackson, and F. Del Rio, Mol. Phys. **97**, 551 (1999).
[40] P. Morgado, H. Zhao, F. J. Blas, C. McCabe, L. P. N. Rebelo, and E. J. M. Filipe, J. Phys. Chem. B **111**, 2856 (2007).
[41] H. Liu, S. K. Kumar, and F. Sciortino, J. Chem. Phys. **127**, 084902 (2007).
[42] Y. Duda, J. Chem. Phys. **130**, 116101 (2009).
[43] Y. Zhou, M. Karplus, K. D. Ball, and R. S. Berry, J. Chem. Phys. **116**, 2323 (2002).
[44] M. P. Allen and D. J. Tildesley, *Computer Simulation of Liquids* (Clarendon, Oxford, 1987).
[45] P. Orea, Y. Duda, and J. Alejandre, J. Chem. Phys. **118**, 5635 (2003).
[46] J. R. Errington, J. Chem. Phys. **118**, 9915 (2003).
[47] A. M. Ferrenberg and R. H. Swendsen, Phys. Rev. Lett. **61**, 2635 (1988).
[48] K. Binder, Phys. Rev. A **25**, 1699 (1982).
[49] J. K. Singh, D. A. Kofke, and J. R. Errington, J. Chem. Phys. **119**, 3405 (2003).
[50] J. K. Singh and D. A. Kofke, J. Chem. Phys. **121**, 9574 (2004).
[51] J. K. Singh, G. Sarma, and S. K. Kwak, J. Chem. Phys. **128**, 044708 (2008).
[52] S. K. Kwak, J. K. Singh, and J. Adhikari, Chemical Product and Process Modeling **2**, 1 (2007).
[53] J. K. Singh, J. Adhikari, and S. K. Kwak, Fluid Phase Equilib. **248**, 1 (2006).
[54] A. N. Kumar and J. K. Singh, Mol. Phys. **106**, 2277 (2008).
[55] A. S. Paluch, V. K. Shen, and J. R. Errington, Ind. Eng. Chem. Res. **47**, 4533 (2008).
[56] J. R. Errington, Phys. Rev. E **67**, 012102 (2003).
[57] L. Vega, E. de Miguel, L. F. Rull, G. Jackson, and I. A. McLure, J. Chem. Phys. **96**, 2296 (1992).
[58] G. Orkoulas and A. Z. Panagiotopoulos, J. Chem. Phys. **110**, 1581 (1999).
[59] See EPAPS Document No. E-JCPSA6-130-037923 for critical properties and surface tension data yielded by the present work. For more information on EPAPS, see http://www.aip.org/pubservs/epaps.html.
[60] S. K. Singh, A. Sinha, G. Deo, and J. K. Singh, J. Phys. Chem. C **113**, 7170 (2009).
[61] J. S. Rowlinson and B. Widom, *Molecular Theory of Capillarity* (Oxford, Oxford, 1982).
[62] I. F. W. Kuo, C. J. Mundy, B. L. Eggimann, M. J. McGrath, J. I. Siepmann, B. Chen, J. Vieceli, and D. J. Tobias, J. Phys. Chem. B **110**, 3738 (2006).
[63] S. W. Sides, G. S. Grest, and M. D. Lacasse, Phys. Rev. E **60**, 6708 (1999).
[64] A. E. Ismail, G. S. Grest, and M. J. Stevens, J. Chem. Phys. **125**, 014702 (2006).
[65] P. Orea, Y. Duda, V. C. Weiss, W. Schröer, and J. Alejandre, J. Chem. Phys. **120**, 11754 (2004).
[66] Y. Reyes-Mercado, P. Orea, S. Lo'pez-Ramirez, and Y. Duda, Physica A **388**, 799 (2009).
[67] N. B. Wilding, J. Phys.: Condens. Matter **9**, 585 (1997).